Accelerated Thermal Simulation for 3D Interactive Optimization of CNC Sheet Metal Laser Cutting

Daniel Mejia
Laboratory of CAD CAM CAE
Universidad EAFIT
Cra 49 no 7-sur-50
050022 Medellín, Colombia
e-mail: dmejiap@eafit.edu.co
e-mail: dmejia@vicomtech.org

Aitor Moreno[*]
Vicomtech-IK4
Paseo Mikeletegi, 57
20009 Donostia/San Sebastián, Spain
e-mail: amoreno@vicomtech.org

Ander Arbelaiz
Vicomtech-IK4
Paseo Mikeletegi, 57
20009 Donostia/San Sebastián, Spain
e-mail: aarbelaiz@vicomtech.org

Jorge Posada
Vicomtech-IK4
Paseo Mikeletegi, 57
20009 Donostia/San Sebastián, Spain
e-mail: jposada@vicomtech.org

Oscar Ruiz-Salguero
Laboratory of CAD CAM CAE
Universidad EAFIT
Cra 49 no 7-sur-50
050022 Medellín, Colombia
e-mail: oruiz@eafit.edu.co

Raúl Chopitea
Lantek Investigación y Desarrollo
Parque Tecnológico de Álava
Ferdinand Zeppelin, 2
01510 Miñano (Araba/Álava), Spain
e-mail: r.chopitea@lantek.es

In the context of CNC-based (Computer Numeric Control) sheet metal laser cutting, the problem of heat transfer simulation is relevant for the optimization of CNC programs. Current physically-based simulation tools use numeric or analytic algorithms which provide accurate but slow solutions due to the underlying mathematical description of the model. This manuscript presents: (1) an analytic solution to the laser heating problem of rectangular plates for curved laser trajectories and convective cooling, (2) a GPU implementation of the analytic solution for fast simulation of the problem, and (3) an integration within an interactive environment for the simulation of sheet metal CNC laser cutting. This analytic approach sacrifices the material removal effect of the laser cut in favor of an approximated real-time temperature map on the sheet metal. The articulation of thermal, geometric and graphic feedback in virtual manufacturing environments enables interactive redefinition of the CNC programs for better product quality, lower safety risks, material waste and energy usage among others. The error with respect to FEA in temperature prediction descends as low as 3.5 %.

Keywords: Computational fabrication, Geometric algorithms, Heat transfer, CNC optimization, Fast simulation

1 Introduction

Sheet metal cutting is an important technique of metalworking, and is widely used in many industries (automotive, aeronautics, etc). One of the most efficient and advanced technologies for sheet metal cutting is CNC laser cutting (specially for steel and aluminum), a process in which a high-power laser beam is directed through a nozzle to cut the material (melting, burning or vaporizing it) providing high-quality surface finishing, greater accuracy, and quicker production [1].

Interactive 3D simulation of CNC laser cuts has proven to be useful at industrial level allowing a better design of the cutting parameters to optimize the production in many ways [2–4]. The ability to interactively visualize and modify the effect of a certain CNC sequence for laser cutting is a valuable resource for manual and automatic optimization procedures that aim to reduce manufacturing costs. Moreover, laser cutting interactive simulation is a good example of the challenges and opportunities identified in [5].

———————
[*]Corresponding Author

However, current laser-cutting interactive simulations are in most cases purely geometric. One of the reasons is the fact that accurate physical simulations require massive computing resources (e.g. FEA), incompatible with interactive simulation.

In this work, we present the implementation of a GPU accelerated simulation of sheet metal laser heating/cutting, integrated into an interactive CNC sheet cut environment. This contribution allows novel and more interactive ways of designing and planning the laser cutting processes, in order to improve not only geometric and material waste aspects, but also the thermal effects on the plate.

The remainder of this manuscript is organized as follows: Section 2 reviews the relevant literature. Section 3 presents the methodology and models used. Section 4 presents and discusses the results. Section 5 presents conclusions and introduces what remains for future work.

2 Literature Review
2.1 Thermal Simulation of Laser Cutting

Analytic solutions to the laser heating problem have been developed in order to estimate the temperature on rectangular plates. Solutions that account only one dimension (distance from the laser source to the hole boundary [6] or the depth of the plate [7]) have been presented for fast solution of laser drilling problems. As the drilling process dictates, such approaches require the laser to be at a fixed location through the entire simulation.

An analytic solution for the 3D laser heating problem is presented in [8]. The solution uses Fourier series to express the temperature field at any location of the plate. However, such solution only accounts for a straight line laser trajectory perpendicular to one of the edges of the rectangular plate. An analytic solution for general piecewise linear laser trajectories is presented in [9]. This approach employs fundamental solutions to compute the temperature on a 3D plate with infinite depth.

Simulation based on analytic solutions provide the advantage of being computationally efficient at the cost of limited model assumptions such as: linear laser trajectories, rectangular domains, constant material properties and null convection on the plate surface [10]. On the other hand, numerical approaches provide stronger tools for the simulation of complex physical phenomena. Finite Element Analysis (FEA) is a common numerical tool for the simulation of thermodynamic phenomena. 3D simulations of triangular [11], rectangular [12, 13] and circular cuts [14] have been achieved using nonlinear FEA to analyze how changes in the laser trajectory impact the resulting temperature profile. To account laser ablation, methodologies such as the element birth and death method [15], volume fractions [16], temperature thresholds [17–19] or the enthalpy method [11–14, 20] are coupled to the FEA routines. Other numerical methods include: Finite Differences [21–24], Boundary Elements [25, 26] and Finite Volumes [27, 28]. All the aforementioned numerical methods present the shortcoming of becoming computationally expensive for large geometries and complex laser trajectories [29–33], rendering them useless for interactive simulation of industrial scenarios.

2.2 Virtual Manufacturing Environment to Support Laser Machining Processes

There has not been a lot of effort in the integration of geometric and physical modules for the simulation of laser machining processes. Current state of the art algorithms for thermal analysis of the problem impose computational time constraints that do not allow an interactive workflow between the geometric simulation and the thermal simulation for complex laser trajectories. However, the integration is a relevant research topic for current trends in virtual manufacturing [5] and specifically, for laser path planning optimization [4, 34]. A coupling of a numerical solver inside a Simulated Annealing program has been presented for the optimization of laser cutting trajectories [23, 35]. The computational cost of such integration is high considering that heuristic algorithms have to simulate multiple thermodynamic scenarios. Therefore, the use of analytical temperature solutions have proven to be more usable for laser path optimization regardless of the underlying model simplifications [36].

To overcome the aforementioned problem, this manuscript presents the integration of a fast analytic heat solver with a geometric module for simulation of the laser cutting process on rectangular plates. The heat solver allows curved laser trajectories and considers convection at the sheet surface. The geometric module represents the sheet using the algorithms described in [3, 37]. The geometric model of the cut sheet is texturized with the color mapped temperature field (dynamically computed in the GPU). The implemented approach allows visual interaction at real-time rates for large geometries and complex laser trajectories.

3 Methodology

This section presents an analytic solution to the laser heating problem on rectangular sheets. The analytic solution enables efficient computation of the temperature for any curved laser trajectory defined on the sheet, allowing convection at the sheet surface. Using the GPU capabilities, the temperature solution is integrated in a geometric module that simulates the CNC machining process and the sheet cutting operation.

3.1 Heat Equation for the Sheet Laser Heating Problem

In the case of a sheet metal, it is reasonable to ignore heat transfer through the plate thickness (i.e. using a 2D model $\nabla \cdot k\nabla = k\frac{\partial^2}{\partial x^2} + k\frac{\partial^2}{\partial y^2}$) due to the relative size of the plate thickness w.r.t. its width and height ($\Delta z \to 0$) and the high thermal conductivity. Therefore, the equation that models the temperature $u = u(\mathbf{x}, t)$ distribution on a 2D rectangular plate subject to a continuous laser source should satisfy
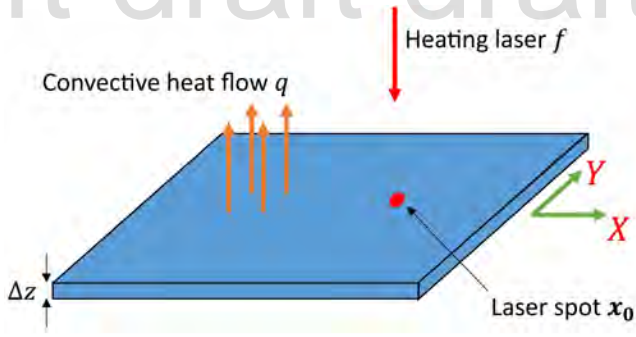
Fig. 1. Schematic of the laser heating model. A laser passes an amount of energy f at a plate location $\mathbf{x_0}$ while the plate cools down due to convection q at the surface.

the following PDE with initial and boundary conditions [38]:

$$\frac{f-q}{\Delta z} = \rho c_p \frac{\partial u}{\partial t} - \nabla \cdot (k\nabla u)$$
$$q = h(u - u_\infty) \tag{1}$$
$$u|_{x=0} = u|_{x=a} = u|_{y=0} = u|_{y=b} = u_\infty$$
$$u(\mathbf{x},0) = u_\infty$$

where ρ, c_p and k are the material density, specific heat and thermal conductivity, respectively (assumed constant in this manuscript). u is the temperature distribution on the plate, q is the heat loss due to convection at the plate surface and f is the surface power density of a squared laser beam centered at $\mathbf{x_0} = [x_0, y_0]$:

$$f(\mathbf{x},\mathbf{x_0}) = \begin{cases} \frac{P(1-R)}{\Delta x^2}, & |x-x_0| < \frac{\Delta x}{2} \quad and \\ & |y-y_0| < \frac{\Delta x}{2} \\ 0, & otherwise \end{cases} \tag{2}$$

with R being theplate reflectivity and P, Δx being the laser power and laser diameter, respectively. The plate initial temperature is assumed at constant ambient temperature u_∞ and the 2D borders of the plate are assumed at ambient temperature for the whole simulation. An scheme of the problem is depicted in Fig. 1.

3.2 Analytic Solution

Similar to [8], the following analytic solution for the temperature distribution can be derived for Eq. (1):

$$u(\mathbf{x},t) = u_\infty + \sum_{i=1}^{\infty}\sum_{j=1}^{\infty} \Theta_{ij}(t)\mathbb{X}_i(x)\mathbb{Y}_j(y) \tag{3}$$

with Fourier basis functions:

$$\mathbb{X}_i(x) = \sin\frac{i\pi x}{a}$$
$$\mathbb{Y}_j(y) = \sin\frac{j\pi y}{b} \tag{4}$$

and their respective Fourier coefficients $\Theta_{ij}(t)$. These Fourier coefficients can be derived using separation of variables:

$$\Theta_{ij}(t_n) = \frac{4}{ab\rho c_p \Delta z}\sum_{l=0}^{n} e^{-\omega_{ij}(t_n - t_l)} \times$$
$$\int_{t_{l-1}}^{t_l}\int_0^b\int_0^a f(\mathbf{x},\mathbf{x_0}(\tau))\mathbb{X}_i(x)\mathbb{Y}_i(y)e^{-\omega_{ij}(t_l-\tau)}dxdyd\tau \tag{5}$$

with eigenvalues ω_{ij} defined as:

$$\omega_{ij} = \frac{k}{\rho c_p}\left(\frac{i^2\pi^2}{a^2} + \frac{j^2\pi^2}{b^2}\right) + \frac{h}{\rho c_p \Delta z} \tag{6}$$

In Eq. (5), the curved trajectory $\mathbf{x_0}(t)$ has been discretized into a piecewise linear trajectory $\mathbf{x_0}(t) = [\mathbf{x_0}(t_0), \mathbf{x_0}(t_1), \cdots, \mathbf{x_0}(t_n)]$. Between the timestep (t_{l-1}, t_l), the linearized laser subtrajectory $\mathbf{x_0}(t_l)$ is defined as:

$$\mathbf{x_0}(t_l) = \mathbf{v}\cdot(t_l - t_{l-1}) + \mathbf{p} \tag{7}$$

with instantaneous speed $\mathbf{v} = [v_x, v_y]^T$ and origin of subtrajectory $\mathbf{p} = [p_x, p_y]^T$. Therefore, for each linear subtrajectory, the integral term in Eq. (5) becomes:

$$\int_{t_{l-1}}^{t_l}\int_0^b\int_0^a f(\mathbf{x},\mathbf{x_0})\mathbb{X}_i(x)\mathbb{Y}_j(y)e^{-\omega_{ij}(t_l-\tau)}dxdyd\tau$$
$$= \frac{abP(1-R)}{ij\pi^2\Delta x^2}$$
$$\left[c_1 c_3 \int_0^{\Delta t} e^{-\omega_{ij}(\Delta t - \tau)}\cos\alpha_x\tau\cos\alpha_y\tau d\tau\right.$$
$$- c_1 c_4 \int_0^{\Delta t} e^{-\omega_{ij}(\Delta t - \tau)}\cos\alpha_x\tau\sin\alpha_y\tau d\tau$$
$$- c_2 c_3 \int_0^{\Delta t} e^{-\omega_{ij}(\Delta t - \tau)}\sin\alpha_x\tau\cos\alpha_y\tau d\tau$$
$$\left.+ c_2 c_4 \int_0^{\Delta t} e^{-\omega_{ij}(\Delta t - \tau)}\sin\alpha_x\tau\sin\alpha_y\tau d\tau\right] \tag{8}$$

where:

$$c_1 = \cos\beta_x - \cos\gamma_x, \quad c_2 = \sin\beta_x - \sin\gamma_x,$$
$$c_3 = \cos\beta_y - \cos\gamma_y, \quad c_4 = \sin\beta_y - \sin\gamma_y,$$
$$\alpha_x = \frac{i\pi v_x}{a}, \quad \alpha_y = \frac{j\pi v_y}{b},$$
$$\beta_x = \frac{i\pi(p_x + \Delta x/2)}{a}, \quad \beta_y = \frac{j\pi(p_y + \Delta x/2)}{b}, \tag{9}$$
$$\gamma_x = \frac{i\pi(p_x - \Delta x/2)}{a}, \quad \gamma_y = \frac{j\pi(p_y - \Delta x/2)}{b}$$
$$\Delta t = t_l - t_{l-1}$$

The integral terms in Eq. (8) can be solved in closed form for any linear subtrajectory, i.e. no numerical integration is required. Therefore, the Fourier solution of the temperature (Eq. (5)) for a given timestep t_l can be computed directly with the available information of (*i*) the sheet and laser parameters, (*ii*) the current linear subtrajectory parameters, and (*iii*) the Fourier solution of the previous timestep t_{l-1}. The temperature of the sheet can be recovered from Eq. (3) after truncating the Fourier solution.

3.3 Interactive Simulation of Thin Metal Plate Cutting

In order to estimate the temperature of the sheet for a given subtrajectory, the analytic algorithm requires (as per Eq. (5)): (*i*) the trajectory of the current machining operation: origin, destination and speed (timing information); and (*ii*) the Fourier coefficients calculated in the previous simulation step. The analytic temperature is estimated by applying the following steps iteratively: (*i*) compute Fourier coefficients for the current subtrajectory, (*ii*) recover the temperature from the computed coefficients.

Configurable discretizations of curved laser trajectories are required. A discretization is basically a piecewise linear reparameterization of a curve $\mathbf{x_0}(t) = [\mathbf{x_0}(t_0), \mathbf{x_0}(t_1), \cdots, \mathbf{x_0}(t_n)]$, which permits variable traversal velocity of the tool and regulation of the torch (power and radius of the laser beam).

In the first step, the calculation of Fourier coefficients for each linear subtrajectory requires only the coefficients from the previous subtrajectory (Eq. (5)). This calculation is fast and independent of the plate geometry discretization. Contrary to FEA methods, Eq. (5) does not impose a restriction on the timestep Δt, allowing arbitrarily large timesteps for any linear subtrajectory.

For the second step, the evaluation of the actual temperatures in the sheet metal requires to use Eq. (3) at discrete sample points of the sheet. A $m \times n$ grid generates such sample points. The temperature evaluated on each sample point is used to create a RGBA color image. A color mapping function is used to obtain a color from a given temperature value.

To simulate the material removal due to laser ablation, the geometric module presented in [3] is used. This geometric module represents the laser trajectory on the sheet as a set of 2D boolean operations between the sheet itself and the contours generated by the laser trajectory. A high-level spatial subdivision algorithm is implemented for such boolean operations in order to increase the computation performance. Moreover, the simulated ablation is purely geometric as the analytic approach does not account for the material removal. This assumption significantly reduces the computational cost of the simulation at the expense of numerical accuracy in the estimated temperature. Such a gain in computational efficiency becomes crucial in industrial applications where immediate albeit approximate results are required for the design of complex CNC processes. Fig. 2 lays out the modules of the CNC laser cut simulator. An additional heat source term might complement Eq. (1) by filtering the heat propagation through the sheet cuts. Such filtering would allow to simulate heat propagation across the empty space produced by the laser cutting process. However, we have not identified any filter of this kind in the literature. Future work aims to explore this possibility.

3.4 Algorithm Analysis

Algorithm 1 presents the pseudocode of the analytic laser cutting simulation. The procedure ANALYTICLASER-SIMULATION calls the analytic routines COMPUTEFOURIER and COMPUTETEMPERATURE.

Algorithm 1 Analytic Simulation of Sheet Laser Cutting

1: **procedure** ANALYTICLASERSIMULATION
2:     $\Theta \leftarrow$ COMPUTEFOURIER($\mathbf{x_0}, num\_coeffs$)
3:     $u \leftarrow$ COMPUTETEMPERATURE(Θ, num_points)
4: **end procedure**
5:
6: **function** COMPUTEFOURIER($\mathbf{x_0}, num\_coeffs$)
7:     Θ.INITIALIZE(num_coeffs)
8:     **for** $\mathbf{x_0}(t_l) \in \mathbf{x_0}$ **do**
9:         **for** $\Theta_{ij} \in \Theta$ **do**
10:             $\Theta_{ij} \leftarrow$ UPDATECOEFFS($\mathbf{x_0}(t_l), \Theta_{ij}$)
11:         **end for**
12:     **end for**
13:     **return** Θ
14: **end function**
15:
16: **function** COMPUTETEMPERATURE(Θ, num_points)
17:     $num\_coeffs \leftarrow \Theta$.SIZE
18:     u.INITIALIZE(num_points)
19:     $x \leftarrow$ SAMPLESHEET(num_points)
20:     **for** $k \in \{0, 1, \ldots, num\_points - 1\}$ **do**
21:         **for** $ij \in \{0, 1, \ldots, num\_coeffs - 1\}$ **do**
22:             $u[k] \leftarrow u[k] +$
23:                 $\Theta_{ij} \times$ FOURIERBASIS$_{ij}(x[k])$
24:         **end for**
25:     **end for**
26:     **return** u
27: **end function**

Given the (piecewise linear) laser trajectory $\mathbf{x_0}$, function COMPUTEFOURIER applies Eq. (5) to compute the Fourier coefficients of the solution. To satisfy $u(\mathbf{x}, t_0) = u_\infty$ in Eq. (3), the Fourier coefficients are initialized by setting $\Theta_{ij}(t_0) = 0$. The calling to function UPDATECOEFFS computes the value of a single Fourier coefficient at the current subtrajectory end given its previous value. Since this last operation is achieved in constant time, the time complexity order of COMPUTEFOURIER is $O(num\_subtrajectories \times num\_coeffs)$.

On the other hand, the function COMPUTETEMPERATURE applies Eq. (3) to retrieve the temperature distribution from the computed Fourier coefficients. The sheet temperature is initialized at ambient temperature (i.e. $u[k] \leftarrow u_\infty$).
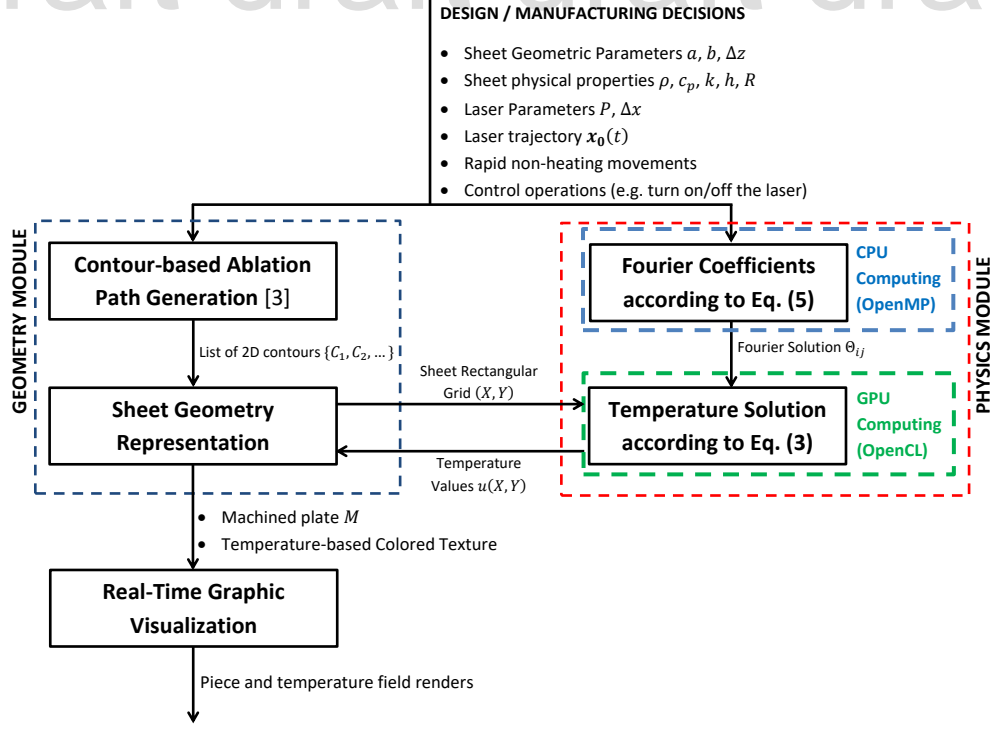
DESIGN / MANUFACTURING DECISIONS

- Sheet Geometric Parameters $a, b, \Delta z$
- Sheet physical properties ρ, c_p, k, h, R
- Laser Parameters $P, \Delta x$
- Laser trajectory $x_0(t)$
- Rapid non-heating movements
- Control operations (e.g. turn on/off the laser)

GEOMETRY MODULE

Contour-based Ablation Path Generation [3]

List of 2D contours $\{C_1, C_2, \dots\}$

Sheet Geometry Representation

Sheet Rectangular Grid (X, Y)

Temperature Values $u(X, Y)$

- Machined plate M
- Temperature-based Colored Texture

Real-Time Graphic Visualization

Piece and temperature field renders

PHYSICS MODULE

Fourier Coefficients according to Eq. (5) — CPU Computing (OpenMP)

Fourier Solution Θ_{ij}

Temperature Solution according to Eq. (3) — GPU Computing (OpenCL)

Fig. 2. Integration scheme between the physics and geometry modules for interactive simulation of the CNC sheet metal laser cutting

The function SAMPLESHEET produces the sheet sampling in linear time $O(num\_points)$. The function FOURIERBASIS applies Eq. (4) to compute the Fourier basis for a given coefficient and a given sample point (in constant time). Therefore, the time complexity order of COMPUTETEMPERATURE is $O(num\_points \times num\_coeffs)$. The infinite sum of Fourier basis functions has been truncated by num_coeffs in order to obtain an approximate solution.

The geometry module call (presented in [3]) simulates the laser cuts on the sheet as geometric boolean operations. Using spatial subdivision, the time complexity order of such calling is $O(ne \times log(ne) + k + z \times log(ne))$ (where z is the number of cut contours, ne is the number of contour edges and k is the number of edge intersections) [3].

As a consequence, the time complexity order of the physical (analytic) module becomes:

$$
O(\text{COMPUTEFOURIER}) + O(\text{COMPUTETEMPERATURE})
$$
$$
= O(ns \times nc) + O(np \times nc)
$$
$$
= O(nc(ns + np))
$$

(10)

with $nc = num\_coeffs$, $ns = num\_subtrajectories$ and $np = num\_points$.

Eqs. (3) and (5) present some interesting properties at the implementation level as follows: 1) for the current sub-trajectory, each Fourier coefficients is independent from the rest of the coefficients and, 2) the temperature at each sample point is independent of the other points. Therefore, the func-

tions COMPUTEFOURIER and COMPUTETEMPERATURE allow easy parallelization. In the following section we take advantage of such parallelization properties in order to use modern parallelization architectures such as multi-core computing and GPU.

4 Results and Discussion

This section presents and discusses the results of the system (Fig. 2) that integrates: *(i)* the physics (analytic) module that calculates the temperature field, and *(ii)* the geometry module for the metal sheet geometry representation. Section 4.1 presents a numerical comparison of our analytic module against a FEA implementation. Section 4.2 presents results of the temperature evaluation using OpenCL. Section 4.3 presents a performance assesment of the analytic module. Section 4.4 discusses the interactivity of our implementation. Section 4.5 discusses the impact of the implemented interactive simulator in the design workflow of CNC-based laser cutting programs.

4.1 Numerical Comparison with FEA

The FEA linear system for Eq. (1) is:

$$
\left[\left(\frac{\rho c_p}{\Delta t} + \frac{h}{\Delta z} \right) \mathbf{M} + k\mathbf{L} \right] \mathbf{U}^{(t+\Delta t)} =
$$
$$
\mathbf{M} \left(\frac{\rho c_p}{\Delta t} \mathbf{U}^{(t)} + \frac{1}{\Delta z} \int_t^{t+\Delta t} \mathbf{F}^{(\tau)} \mathrm{d}\tau + \frac{h}{\Delta z} u_\infty \right)
$$

(11)

Table 1. Physical parameters for simulation of laser heating of an AISI 304 steel plate with natural convection at the surface [39]

Parameter	Value
ρ	$8030\,kg/m^3$
c_p	$574\,J/(kg \cdot K)$
k	$20\,W/(m \cdot K)$
R	0
h	$20\,W/(m^2 \cdot K)$
u_∞	$300\,K$

where:

$$\mathbf{L}_{ij} = \sum_{\Omega_k \in \Omega} \int_{\Omega_k} \nabla \phi_i \cdot \nabla \phi_j \mathrm{d}A$$

$$\mathbf{M}_{ij} = \sum_{\Omega_k \in \Omega} \int_{\Omega_k} \phi_i \phi_j \mathrm{d}A \tag{12}$$

are the stiffness and mass matrices, respectively. $\Omega = \{\Omega_1, \Omega_2, \ldots, \Omega_m\}$ is a discretization of the plate into finite elements. $\mathbf{X} = \{\mathbf{x}_1, \mathbf{x}_2, \ldots, \mathbf{x}_n\}$ is the discrete set of mesh nodes. $\phi_i = \phi_i(\mathbf{x})$ is the interpolation function associated to the node $\mathbf{x}_i$. $\mathbf{U}^{(t)} = [u(\mathbf{x}_1, t), u(\mathbf{x}_2, t), \ldots, u(\mathbf{x}_n, t)]^T$ and $\mathbf{F}^{(t)} = [f(\mathbf{x}_1, t), f(\mathbf{x}_2, t), \ldots, f(\mathbf{x}_n, t)]^T$ are the nodal values of the temperature and the laser source, respectively. Δt is the simulation timestep.

A case is studied contrasting *(a)* analytic and *(b)* FEA implementations. The case conditions are:

1. Sheet geometry: $0.01\,m \times 0.01\,m \times 0.001\,m$.
2. Material: AISI 304 steel (Table 1).
3. Laser power: $100\,W$.
4. Laser spot radius: $r = 0.0003\,m$.
5. Traversal laser speed: $0.1\,m/s$.

The laser beam follows an S-shape trajectory. A timestep $\Delta t = 0.0012\,s$ is chosen for the FEA time discretization.

Fig. 3(a) plots the plate temperature distribution at the end of the analytic simulation ($t = 0.12\,s$) using 100×100 Fourier coefficients. Fig. 3(b) shows the relative error distribution of the analytic model considering the FEA solution as reference. The maximal relative error (3.43%) occurs at the laser spot. Additional experiments increasing the number of Fourier coefficients did not provide any significant improvement in the analytic solution of the current study case.

Domains with sizes above the small one here discussed do not permit termination of the FEA computation. Therefore, a comparison analytic vs. FEA is only possible for exceedingly small domains. Following subsections present study cases with larger domains.

4.2 Temperature Evaluation Assisted by GPU

The analytic approach presented in section 3, permits a parallel implementation, which this section discusses. As
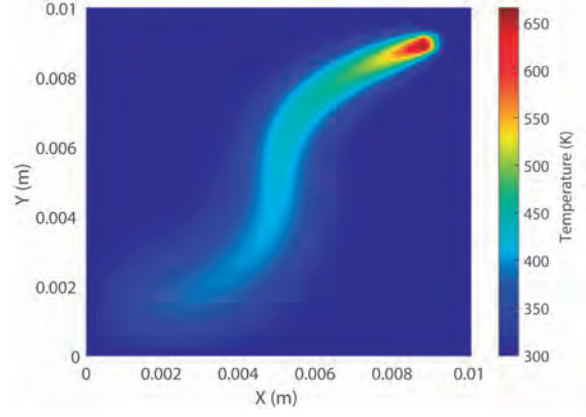
(a) Analytic temperature distribution at $t = 0.12\,s$
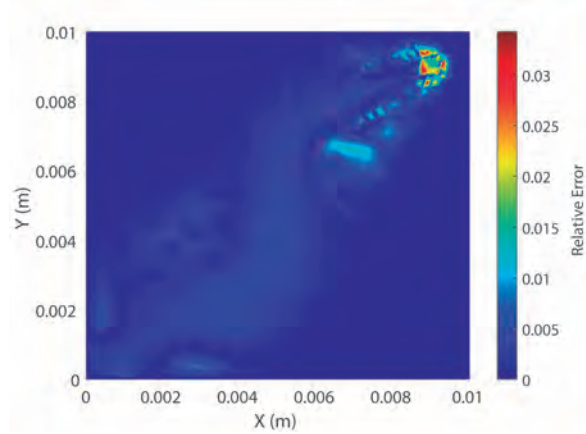
(b) Relative error. Analytic vs. FEA solution. Relative error below 3.43%

Fig. 3. Analytic temperature and relative error distribution (w.r.t. FEA) for the S-shape laser trajectory

specified in section 3.3, grid sampling is used in order to obtain the temperature at discrete points on the sheet. To illustrate the capabilities of the presented approach, a study case with complex laser trajectory is evaluated on a large (larger than FEA) sheet metal. The following setup is used:

1. Sheet geometry: $0.235\,m \times 0.235\,m \times 0.01\,m$.
2. Material: AISI 304 steel (Table 1).
3. Laser power: $8000\,W$.
4. Laser spot radius: $r = 0.0001\,m$.

The study presents a custom CAM model to produce a set of nested squares. The resulting CNC program is composed as a combination of cutting and non-cutting instructions:

1. **Machining instructions:** Instructions which move the laser head and cut the sheet. The laser moves at traversal speed $\|\vec{v}\| = 0.028\,m/s$.
2. **Rapid non-cutting movements:** Instructions which move the laser head but do not cut the sheet ($P = 0\,W$). The laser moves at traversal speed $\|\vec{v}\| = 0.183\,m/s$.
3. **Other CNC control instructions:** Sourceless ($P = 0\,W$) and static ($\|\vec{v}\| = 0\,m/s$) instructions (such as pow-
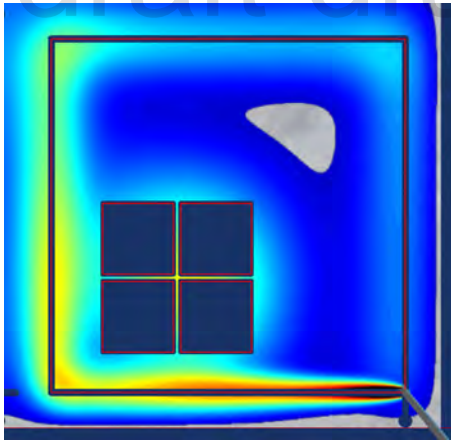
(a) Temperature texture map
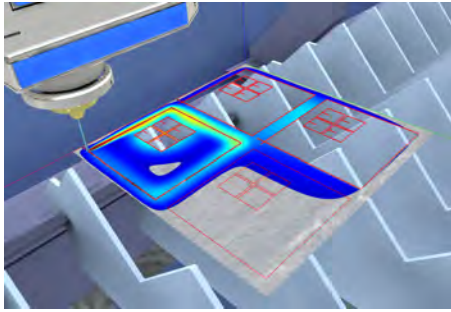
(b) Visualization of the cutting process in the interactive simulator

Fig. 4. Simulation of the CNC process integrating the physical (512×512 Fourier coefficients) and the geometric modules (1024×1024 grid points)

ering on and off the laser beam) simulated as delays of $1s$.

As illustrated in section 3.4, the computation time of our analytic algorithm is determined by the number of Fourier coefficients times the number of sample points, which for high Fourier and sampling resolutions may render our algorithm beyond the interactivity needs. However, evaluation of the sheet temperature is independent for each sampling point (as per Eq. (3)), thus the temperature distribution can be easily evaluated in parallel. Therefore, the computation time of the temperature becomes determined by the number of coefficients, which ultimately translates to a great amount of memory access operations. Unlike CPUs, current GPUs can evaluate a larger number of sample points in parallel and provide faster and more efficient memory access. In definitive, GPUs are better suited for the temperature evaluation problem. Therefore, a GPGPU implementation of Eq. (3) has been developed using OpenCL [39] as follows: (*1*) The Fourier coefficients are transferred from host memory to the GPU memory. (*2*) A 1D OpenCL kernel is launched to perform the temperature evaluation. The number of threads is determined by the desired number of sample points (resolution), the local work-group size is determined by the underlying OpenCL implementation in function of the GPU. (*3*) When the kernel computation finalizes the results are trans-

ferred from GPU to host memory.

The simulation system is implemented in a Windows 10 platform using C++ with OpenMP support. OpenCL support is provided by the NVIDIA native drivers through the proprietary CUDA API. With a grid sampling of 512×512 and 512×512 coefficients, the temperature evaluation takes about $1.59s$ in average (without considering the computation times of the Fourier coefficients) for any given subtrajectory. Increasing the number of coefficients or the number of sampling points increases linearly the temperature evaluation times (see Table 2). Fig. 4 plots the temperature distribution at the middle of the sheet laser cutting simulation, coupling both the analytic and the geometric modules.

The number of coefficients and grid resolution cannot be increased without limit, as the internal GPU memory, registers and available threads are finite. In our test machine (Table 3) increasing the grid resolution and number of coefficients above 2048×2048 and 1024×1024 respectively, reduces significantly our GPU performance, rendering noncomputable results beyond such resolutions (as shown in Table 2 where such combination crashes the GPU computation).

In order to compute the temperature, the Fourier coefficients must be calculated as per Eq. (5). The independence between Fourier coefficients allows efficient CPU parallelization of this calculation using OpenMP. Fig. 5 plots the computation times of the Fourier coefficients for different Fourier resolutions. Such calculation could be implemented directly in the GPU. However, our experiments show that the CPU times are fast enough to allow the interactivity rate (below 0.15 seconds for the larger resolution).

4.3 Assessment of Computing Performance

Table 4 presents CPU (with OpenMP support) performance results for the temperature calculation of the test case introduced in section 4.2. Compared to the GPU results (red see Table 2), the CPU implementation shows significant performance decrease. As an example, the 256×256 test case (0.102 seconds) runs 150 times faster than the CPU execution (15.877 seconds). As a rule of thumb, we consider interactive simulation if the waiting times for the user lie below 5 seconds. The CPU implementation breaks this rule of thumb for moderate resolutions (up to 128×128 Fourier coefficients and 256×256 grid points) while the GPU allows larger resolutions (up to 256×256 Fourier coefficients and 1024×1024 grid points).

In addition, linear FEA for thermal analysis has been implemented in MATLAB with adaptive re-meshing from the MATLAB PDE Toolbox in order to compare the performance between FEA and our analytic (GPU) algorithm. Since FEA simulation becomes unfeasible as the sheet size increases and the laser trajectory becomes more complex [29, 33], the (much smaller) test case presented in section 4.1 is used for such comparison. In our test machine (red see Table 3), the FEA computation of the temperature for a sheet discretization of 3586 points and 100 simulation timesteps takes in average 6.3835 seconds (not considering FEA re-

Table 2. GPU implementation. Execution times (in seconds) for retrieving the temperature at a given timestep t_l, according to Eq. (3). Computation times of Fourier coefficients are not considered.

Fourier Coeffs. \ Grid Resolution	64×64	128×128	256×256	512×512	1024×1024	2048×2048	4096×4096
64×64	0.001313	0.002641	0.007977	0.029518	0.115439	0.4318	1.6787
128×128	0.002796	0.008041	0.027954	0.110535	0.414949	1.6098	6.3809
256×256	0.008013	0.027058	0.101933	0.415542	1.591032	6.3067	25.1822
512×512	0.028004	0.101988	0.397375	1.598041	6.281901	25.0937	100.3546
1024×1024	0.105995	0.401026	1.581736	6.327188	25.08374	100.3443	N/A

Table 3. Modest hardware and software specifications of the machine used to run the the CNC simulations

Item	Specifications
Operating System	Microsoft Windows 10 Pro (64 bits)
Processor	Intel©Core™i5-6500 CPU @3.20GHz
RAM	8.0 GB
GPU	NVIDIA GeForce GTX 960
OpenCL	OpenCL 1.2 CUDA 8.0.0
Compilation Environment	Visual Studio 2013™(x64 with optimization -O2 flags)

Table 4. CPU implementation. Execution times (in seconds) for the computation of the temperature at a given timestep t_l, according to Eq. (3).

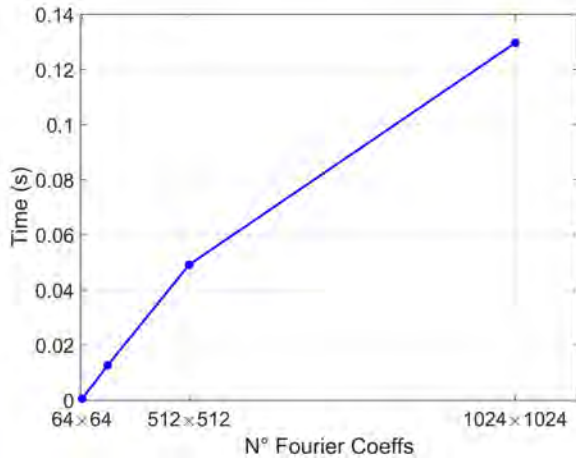| Fourier Coeffs. \ Grid Res.	64×64	128×128	256×256	512×512
64×64	0.0662	0.2630	1.0169	3.9880
128×128	0.2771	1.0788	4.3264	16.8444
256×256	1.1368	4.0004	15.8775	63.9231
512×512	3.9514	15.5803	62.5949	250.4050

Fig. 5. CPU computation times of the Fourier coefficients for a single timestep (as per Eq. (5))

meshing time). In contrast, our GPU implementation of the analytic algorithm performs the same trajectory simulation (with 100×100 Fourier coefficients) in 0.3556 seconds (18 times faster).

4.4 Interactive Simulation of the Laser Cutting Process

Our work efficiently integrates geometry and thermal modules for the simulation of sheet metal CNC laser cut. We use a contour-based representation to model the geometry of the processed sheet [3, 37], coupled with an analytic solution of the underlying thermal phenomena which generates the corresponding temperature texture. The simulator presents the user a virtual 3D interactive scenario with a fully detailed CNC machine equipped with a virtual laser that will be the target of the machining instructions. In this virtual scene, the metal sheet is rendered with the computed temperature distribution on its surface.

We identify two different use cases in the virtual 3D simulator: *(1)* the user visualizes the machining simulation as a continuous animation to track the overall process and, *(2)* the user inspects a specific timestep of the simulation looking for more detail in the current state of the sheet (e.g. cutting and temperature profile near the laser spot).

In the first scenario, the temperature on the plate plate is calculated after each machining movement. Even if some preprocessing must be done, the worst case scenario implies a user request of the whole process as soon as the simulator itself is loaded. The computation process involves the utilization of CPU and GPU resources. The contour-based representation is calculated in the CPU (single-threaded). For each machining instruction, a new updated geometric representation of the metal sheet is generated. At the same time, the Fourier coefficients are calculated in CPU using all its available cores (thanks to OpenMP). Once the geometry and the coefficients are calculated, the temperature field is evaluated in the GPU using a 256×256 grid with 300×300 Fourier coefficients (thanks to OpenCL). This grid resolution is small enough to allow fast and interactive visualization of the machining process (below $0.12 s$. as shown in Table 2).

In the second scenario, the simulation is stopped at a given timestep and the user interactively inspects the current state of the machining process. In this scenario, the user might request a more accurate representation of the temperatures on the metal plate. In such case, the computing time is less penalized in favor of more precise results. Some UI elements enable the user to configure the desired quality of these results. Therefore, if high quality is requested, a 1024×1024 grid sampling is used with 1024×1024 Fourier coefficients. This combination of grid resolution and number of coefficients provide high quality results and it is dependent on the existing GPU hardware. State-of-the-art GPU models might use 2048×2048 or higher grid resolutions within affordable computational time limits (below 5-6 s).

4.5   Impact in the Design Workflow of CNC Programs

The design process of CNC programs is essentially iterative. The designer receives the list of parts to be produced, their material and any other relevant information. The nesting software produces the arrangement of the parts in any of the available metal sheets in the Manufacturing Execution System (MES) software. This process can be configured by the designer in order to optimize different aspects of the machining process such as: *i)* minimization of the produced scrap, *ii)* minimization of the overall machining time and *iii)* reduction of rapid movements over cut parts (to reduce potential collisions).

As a consequence, professional nesting software provides a variety of options to the designer to fine-tune the produced CNC program. This number of options continuously increases. Therefore, an analysis of different simulated scenarios aids the designer in the parameter selection of the CNC machine for an optimal configuration. As an example, the energy output of the laser must be controlled. The available laser with the highest power is not always the best option to operate in the metal sheet. It might produce better quality cuts with positive economical consequences (such as less machining time), negative economical consequences (such as more energy consumption) or potential side-effects in the quality of the parts near the cut zone. Therefore, the selection of the proper heat source parameters can be optimized with the support of the CNC simulator.

Using high quality simulations with FEA software is precise but computationally expensive [29–33]. Therefore, the number of test scenarios to be carried out during the design phase becomes limited. On the other hand, utilization of fast simulation software like the one presented in this work, enables the simulation of a considerable number of test scenarios. The design workflow would be more agile and versatile, providing new optimization opportunities that would led to better CNC programs in terms of quality of the parts, economical benefits, wasted resources and safety of the operators in the factory floor.
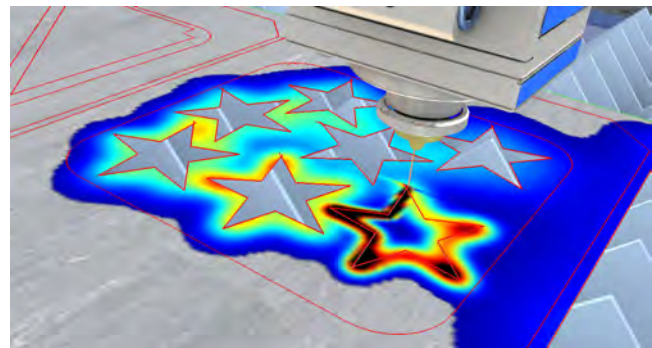
Fig. 6 shows the metal sheet cutting simulator running a real CNC program. The temperature texture on the sheet surface provides useful information to the designer. As an example, heat progation around the recent cut part (star) af-
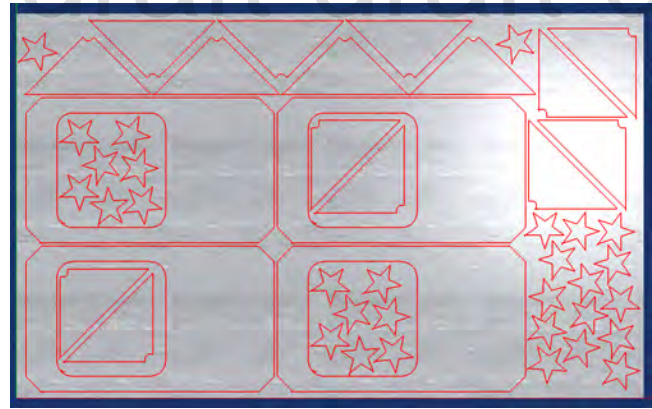
(a) Nesting of the CNC program
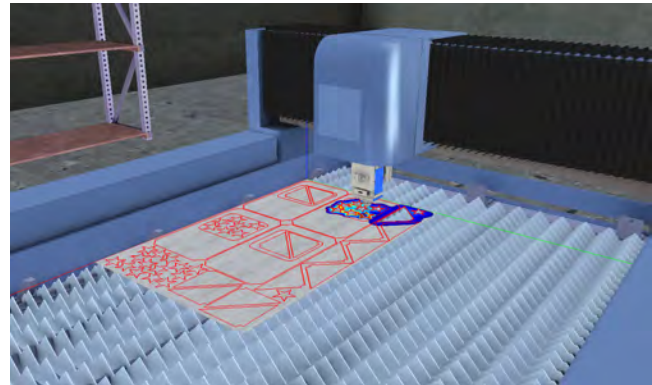
(b) Overall 3D visualization of the CNC simulation

(c) Detailed inspection near a recent cut. Heat affects posterior cuts.

Fig. 6.   The interactive CNC simulator can be used to detect potential problems in the nesting planning due to heat propagation

fects posterior cuts (Fig. 6(c)). Therefore, the designer might consider to modify the arrangement of the star cuts in order to reduce potential rejections of the produced parts in the post-machining inspection.

5   Conclusions and Future Work

This manuscript implements an integration of a physical and a geometric module for fast and interactive simulation of CNC-based sheet metal laser cutting.

Sections 3.1 and 3.2 presents the analytic solution to the laser heating problem. Although the assumptions of the mathematical model simplify the laser heating phenomenon (constant material properties, no material removal, no phase

changes and constrained sheet geometries), the analytic algorithm provides an efficient solution to problems that are very expensive computationally for current FEA methods.

Section 3.3 presents the integration of the geometric and physic modules in the CNC simulator. A grid sampling of the metal sheet is used to calculate the temperature distribution and to create a texture that will be overlaid on the geometric representation of the sheet. The goal of the grid sampling is to provide fast and detailed results for visual inspection at an specific timestep using the GPU. A complexity analysis of the analytic approach is presented in section 3.4. The parallelization properties of the mathematical description allow efficient implementation of the algorithm.

A numerical comparison with FEA is presented in section 4.1. With the curved *S* trajectory path case, the calculated maximum error is 3.43% around the laser spot.

Section 4.2 presents the results for the integrated CNC simulator with the grid sampling technique. The implementation of Equation (3) in OpenCL allows the utilization of the capabilities of modern GPU hardware to speed up the temperature calculation. Section 4.3 conducts a performance assesment of such GPU implementation against non-GPU analytic implementation and FEA. The GPU implementation performs 150 times faster than the CPU implementation and 18 times faster than linear FEA, allowing our approach to run interactive simulations of complex CNC programs, which are otherwise non-computable in the latter ones.

The analytic model presented in section 3 simplifies by design the thermal phenomena of laser cutting in order to achieve real-time performance. As future work, we aim to (1) introduce nonlinear physical behaviour into the analytical model in the form of nonlinear material properties and material ablation (sheet removal), (2) evaluate the accuracy of the method with experimental data in order to provide error bounds, and (3) use meshing techniques that improve the sheet sampling in order to allow even larger sheet configurations and better temperature resolutions near the laser spot.

Acknowledgements

References

[1] Steen, W. M., and Mazumder, J., 2010. *Laser Cutting, Drilling and Piercing*. Springer London, London, pp. 131 – 198.

[2] Spence, A. D., and Li, Z., 2001. "Parallel processing for 2-1/2d machining simulation". In Proceedings of the Sixth ACM Symposium on Solid Modeling and Applications, SMA '01, ACM, pp. 140–148.

[3] Moreno, A., Segura, Á., Arregui, H., Posada, J., Ruíz de Infante, Á., and Canto, N., 2014. *Using 2D Contours to Model Metal Sheets in Industrial Machining Processes*. Springer London, London, pp. 135–149.

[4] Dewil, R., Vansteenwegen, P., and Cattrysse, D., 2016. "A review of cutting path algorithms for laser cutters". *The International Journal of Advanced Manufacturing Technology,* **87**(5), pp. 1865 – 1884.

[5] Posada, J., Toro, C., Barandiaran, I., Oyarzun, D., Stricker, D., de Amicis, R., Pinto, E. B., Eisert, P., Dllner, J., and Vallarino, I., 2015. "Visual computing as a key enabling technology for industrie 4.0 and industrial internet". *IEEE Computer Graphics and Applications,* **35**(2), Mar, pp. 26 – 40.

[6] Modest, M., and Abakians, H., 1986. "Evaporative cutting of a semi-infinite body with a moving CW laser". *J. Heat Trans. - T. ASME,* **108**(3), pp. 602 – 607.

[7] Zimmer, K., 2009. "Analytical solution of the laser-induced temperature distribution across internal material interfaces". *Int. J. Heat Mass Trans.,* **52**(1-2), pp. 497 – 503.

[8] Jiang, H.-J., and Dai, H.-L., 2015. "Effect of laser processing on three dimensional thermodynamic analysis for HSLA rectangular steel plates". *Int. J. Heat Mass Trans.,* **82**, pp. 98 – 108.

[9] Winczek, J., 2010. "Analytical solution to transient temperature field in a half-infinite body caused by moving volumetric heat source". *Int. J. Heat Mass Trans.,* **53**(25-26), pp. 5774 – 5781.

[10] Parandoush, P., and Hossain, A., 2014. "A review of modeling and simulation of laser beam machining". *Int. J. Mach. Tool. Manu.,* **85**, pp. 135 – 145.

[11] Yilbas, B., Akhtar, S., and Keles, O., 2014. "Laser cutting of triangular blanks from thick aluminum foam plate: Thermal stress analysis and morphology". *Appl. Therm. Eng.,* **62**(1), pp. 28 – 36.

[12] Akhtar, S., Kardas, O., Keles, O., and Yilbas, B., 2014. "Laser cutting of rectangular geometry into aluminum alloy: Effect of cut sizes on thermal stress field". *Opt. Laser Eng.,* **61**, pp. 57 – 66.

[13] Yilbas, B., Akhtar, S., and Karatas, C., 2014. "Laser cutting of rectangular geometry into alumina tiles". *Opt. Laser Eng.,* **55**, pp. 35 – 43.

[14] Akhtar, S., 2014. "Laser cutting of thick-section circular blanks: thermal stress prediction and microstructural analysis". *Int. J. Adv. Manuf. Tech.,* **71**(5), pp. 1345 – 1358.

[15] Roberts, I., Wang, C., Esterlein, R., Stanford, M., and Mynors, D., 2009. "A three-dimensional finite element analysis of the temperature field during laser melting of metal powders in additive layer manufacturing". *Int. J. Mach. Tool. Manu.,* **49**(12-13), pp. 916 – 923.

[16] Shi, B., and Attia, H., 2013. "Integrated process of laser-assisted machining and laser surface heat treatment". *J. Manuf. Sci. Eng.,* **135**(6).

[17] Akarapu, R., Li, B., and Segall, A., 2004. "A thermal stress and failure model for laser cutting and forming operations". *Journal of Failure Analysis and Prevention,* **4**(5), pp. 51 – 62.

[18] Nyon, K., Nyeoh, C., Mokhtar, M., and Abdul-Rahman, R., 2011. "Finite element analysis of laser inert gas cutting on inconel 718". *Int. J. Adv. Manuf.*

Tech., **60**(9), pp. 995 – 1007.

[19] Fu, C., Sealy, M., Guo, Y., and Wei, X., 2015. "Finite element simulation and experimental validation of pulsed laser cutting of nitinol". *Journal of Manufacturing Processes,* **19**, pp. 81 – 86.

[20] Yilbas, B., Akhtar, S., and Keles, O., 2013. "Laser cutting of aluminum foam: Experimental and model studies". *J. Manuf. Sci. Eng.,* **135**(5).

[21] Modest, M., 1996. "Three-dimensional, transient model for laser machining of ablating/decomposing materials". *Int. J. Heat Mass Trans.,* **39**(2), pp. 221 – 234.

[22] Modest, M., 1997. "Laser through-cutting and drilling models for ablating/decomposing materials". *J. Laser Appl.,* **9**(3), pp. 137 – 145.

[23] Han, G., and Na, S., 1999. "A study on torch path planning in laser cutting processes part 1: Calculation of heat flow in contour laser beam cutting". *J. Manuf. Syst.,* **18**(2), pp. 54 – 61.

[24] Xu, W., Fang, J., Wang, X., Wang, T., Liu, F., and Zhao, Z., 2005. "A numerical simulation of temperature field in plasma-arc forming of sheet metal". *J. Mater. Process. Tech.,* **164 - 165**, pp. 1644 – 1649.

[25] Kim, M., 2000. "Transient evaporative laser-cutting with boundary element method". *Appl. Math. Model.,* **25**(1), pp. 25 – 39.

[26] Kim, M., 2004. "Transient evaporative laser cutting with moving laser by boundary element method". *Appl. Math. Model.,* **28**(10), pp. 891 – 910.

[27] Kheloufi, K., Hachemi, A., and Benzaoui, A., 2015. "Numerical simulation of transient three-dimensional temperature and kerf formation in laser fusion cutting". *J. Heat Trans. - T. ASME,* **137**(11).

[28] Yuan, P., and Gu, D., 2015. "Molten pool behaviour and its physical mechanism during selective laser melting of TiC/AlSi10Mg nanocomposites: simulation and experiments". *J. Phys. D. - Appl. Phys.,* **48**(3), p. 035303.

[29] Gross, M. S., 2006. "On gas dynamic effects in the modelling of laser cutting processes". *Appl. Math. Model.,* **30**(4), pp. 307 – 318.

[30] Boffy, H., Baietto, M., Sainsot, P., and Lubrecht, A., 2012. "Detailed modelling of a moving heat source using multigrid methods". *Tribol. Int.,* **46**(1), pp. 279 – 287.

[31] Gupta, N., and Nataraj, N., 2013. "A posteriori error estimates for an optimal control problem of laser surface hardening of steel". *Adv. Comput. Math.,* **39**(1), pp. 69 – 99.

[32] Bailey, N., Tan, W., and Shin, Y., 2013. "A parametric study on laser welding of magnesium alloy AZ31 by a fiber laser". *J. Manuf. Sci. Eng.,* **137**(4).

[33] Mejia, D., Moreno, A., Ruiz-Salguero, O., and Barandiaran, I., 2016. "Appraisal of open software for finite element simulation of 2d metal sheet laser cut". *International Journal on Interactive Design and Manufacturing (IJIDeM)*, pp. 1 – 12.

[34] Kim, H., Lee, S., and Yang, D., 2009. "Toolpath planning algorithm for the ablation process using energy

sources". *Computer-Aided Design,* **41**(1), pp. 59 – 64.

[35] Han, G.-C., and Na, S.-J., 1999. "A study on torch path planning in laser cutting processes part 2: Cutting path optimization using simulated annealing". *Journal of Manufacturing Systems,* **18**(2), pp. 62 – 70.

[36] Kim, Y., Gotoh, K., and Toyosada, M., 2004. "Global cutting-path optimization considering the minimum heat effect with microgenetic algorithms". *Journal of Marine Science and Technology,* **9**(2), pp. 70 – 79.

[37] Velez, G., Moreno, A., Infante, A. R. D., and Chopitea, R., 2016. "Real-time part detection in a virtually machined sheet metal defined as a set of disjoint regions". *International Journal of Computer Integrated Manufacturing,* **29**(10), pp. 1089–1104.

[38] Pietro, P. D., and Yao, Y., 1995. "A numerical investigation into cutting front mobility in CO2 laser cutting". *Int. J. Mach. Tool. Manu.,* **35**(5), pp. 673 – 688.

[39] Yilbas, B., and Akhtar, S., 2014. "Laser bending of metal sheet and thermal stress analysis". *Opt. Laser Technol.,* **61**, pp. 34 – 44.